

Guided Transfer Learning for Discrete Diffusion Models

Julian Kleutgens^{1,2}, Claudio Battiloro¹, Lingkai Kong¹, Benjamin Grewe², Francesca Dominici¹,
Mauricio Tec¹

¹Harvard University

²ETH Zürich

Abstract

Discrete diffusion models achieve strong performance across language and other discrete domains, providing a powerful alternative to autoregressive models. However, their strong performance relies on large training datasets, which are costly or risky to obtain, especially when adapting to new domains. Transfer learning is the natural way to adapt pretrained discrete diffusion models, but current methods require fine-tuning large diffusion models, which is computationally expensive and often impractical. Building on ratio-based transfer learning for continuous diffusion, we provide Guided Transfer Learning for discrete diffusion models (GTL). This enables sampling from a target distribution without modifying the pretrained denoiser. The same guidance formulation applies to both discrete-time diffusion and continuous-time score-based discrete diffusion, yielding a unified treatment. Guided discrete diffusion often requires many forward passes of the guidance network, which becomes impractical for large vocabularies and long sequences. To address this, we further present an efficient guided sampler that concentrates evaluations on planner-selected positions and top candidate tokens, thus lowering sampling time and computation. This makes guided language modeling practical at scale for large vocabularies and long sequences. We evaluate GTL on sequential data, including synthetic Markov chains and language modeling, and provide empirical analyses of its behavior. **This is a pre-print.**

1 Introduction

Diffusion models (Ho, Jain, and Abbeel 2020; Song et al. 2021) have become the dominant approach for generative modeling in continuous domains like image, video, and audio (Lovelace et al. 2023; Ho et al. 2022; Liu et al. 2023). More recently, discrete diffusion models for language have achieved competitive performance and, by denoising tokens in parallel and in any order, offer practical advantages for controllable infilling and editing compared to left-to-right autoregressive decoding (Gong et al. 2025; Li et al. 2022a). Among existing discrete diffusion approaches, masked diffusion models (MDMs) have demonstrated remarkable performance in tasks such as reasoning (Nie et al. 2025; Zheng et al. 2025), planning (Ye et al. 2025), and infilling (Gong et al. 2025), often performing on par with state-of-the-art auto-regressive language models (ALMs).

An open problem in the field is to develop transfer learn-

ing approaches that enable leveraging the incredible performance of large pre-trained diffusion models in domains with scarce data (Ouyang et al. 2024). In the continuous domain, recent works have explored transfer learning approaches based domain classifiers (ratio estimators) (Zhong et al. 2025; Ouyang et al. 2024). Such methods bypass the need of updating millions of parameters, providing an alternative to adapter-based finetuning (Moon et al. 2022; Xie et al. 2023) and reinforcement learning (Fan et al. 2023; Clark et al. 2024) in scenarios of extreme scarcity.

In this paper, we tackle the problem of extending domain classifier-based sampling for discrete diffusion models. We first develop the theoretical analogues of (Ouyang et al. 2024), leading to a first naïve implementation of (8) (In supplementary materials, algorithm 2). However, we show that such naïve implementation requires $\mathcal{O}(L|\mathcal{V}|)$ guidance evaluations per denoising step, scaling poorly with sequence length L and vocabulary size $|\mathcal{V}|$, limiting its applicability to domains such as language modeling.

Motivated by these challenges, we introduce Guided Transfer Learning (GTL) for discrete diffusion models. Our method leverages a pretrained source discrete diffusion model and introduces a compact ratio network that estimates the density ratio between the target and source data distributions. We demonstrate that sampling from the target domain can be achieved solely by training this ratio-based guidance module, enabling effective target sampling without updating the denoiser. This substantially reduces the training cost compared to conventional fine-tuning approaches. We establish a closed-form solution for the sampling method, and we further extend this argument to continuous-time score-based models. This generalization allows our approach to cover the two dominant diffusion frameworks: score-based models (Lou, Meng, and Ermon 2024; Sun et al. 2023) and discrete-time diffusion models (Austin et al. 2023), making the method broadly applicable to diffusion modeling. This GTL construction does not follow directly from continuous diffusion models (Ouyang et al. 2024), since score-matching diffusion is not defined for categorical discrete tokens and cannot be derived from the score-matching loss function (Song et al. 2021). We further introduce a guided sampling algorithm that reduces the number of guidance calls per denoising step by focusing computation on planner-selected tokens. This design improves efficiency. Previewing

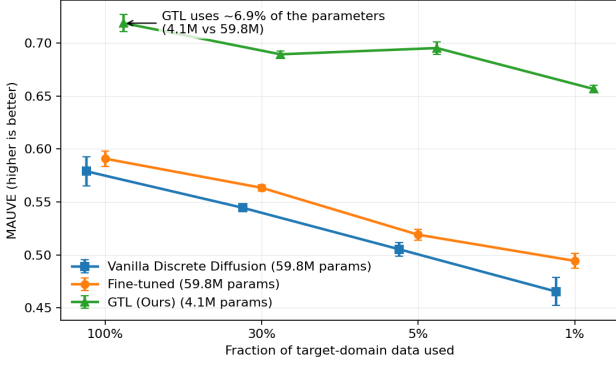


Figure 1: *GTL outperforms with 7% of the parameters.* MAUVE (\uparrow) vs. fraction of target-domain training data (e.g., 100% = all 79,631 arXiv Physics abstracts; 1% \approx 800). Our Guided Transfer Learning (GTL, green) achieves the highest MAUVE across all data regimes while training only a 4.1M parameter ratio model outperforming both Vanilla (trained only on target data) and Fine-tuned (source-pretrained then fine-tuned on target) models. Points show mean, and error bars show standard error over 3 \times 3 (train \times sample) seeds. See Section 5.2 for the experimental setup and evaluation details.

our results, GTL surpasses vanilla and fine-tuned diffusion across all data-scarcity regimes while training only 7% as many parameters (Fig. 1).

We summarize our contributions as follows:

1. We introduce GTL, an effective transfer learning framework for discrete diffusion models. GTL keeps the source denoiser fixed while training a lightweight ratio estimator on both source and target data to enable sampling from the target distribution. GTL achieves scalability by using an unmasking position for the top- n_{ratio} candidates, dramatically reducing the per-step computational cost, without sacrificing performance in practice.
2. We provide a theoretical analysis and formal theorem of the proposed guided transfer learning method, demonstrating that ratio-based guidance correctly recovers the target reverse transition.
3. We validate GTL and the guided sampler on sequential data, including synthetic Markov chains and arXiv abstract language modeling tasks.

2 Related Work

Discrete Diffusion Models Discrete diffusion models (DDMs) are widely used for biological sequence generation (e.g., DNA, RNA, proteins) as well as language modeling (Sarkar et al. 2024; Yu, Li, and Wang 2025). Continuous-noise variants that corrupt embeddings or latents are likely to suffer from embedding-to-token projection mismatch (Li et al. 2022b; Lovelace et al. 2023). Beyond that, two widely adopted formulations operate entirely in discrete space, avoiding continuous mappings. First, simplified masked diffusion models such as MLDM and MD4

follow the D3PM framework, using discrete-time transition matrices with a denoiser trained to invert the forward kernels (Sahoo et al. 2024; Shi et al. 2025; Austin et al. 2023). Second, continuous-time discrete diffusion estimates a discrete score, which represents the log-ratio between adjacent-timestep marginals. This induces a continuous-time Markov chain (CTMC) (Lou, Meng, and Ermon 2024; Meng et al. 2023; Campbell et al. 2022).

Guided Diffusion Models In both continuous and discrete settings, guidance strategies like classifier-based or classifier-free are widely used. In the discrete case, classifier-free guidance typically performs two forward passes at inference time, one conditional and one unconditional, while training a single large model on a mixture of conditional prompt-input pairs and unconditional data (Huang and Tang 2025). Closer to our approach is classifier-based guidance, which steers generation using a classifier $p(y | x_t, t)$ while the denoiser is trained on the full corpus; sampling is biased toward the target label y in the data distribution (Schiff et al. 2025; Nisonoff et al. 2025). In both discrete- and continuous-time formulations, this typically yields per-token factorized guidance, which incurs many computational steps, scaling with $\mathcal{O}(L|\mathcal{V}|)$ evaluations per denoising step. To mitigate this cost, (Nisonoff et al. 2025) proposes a first-order Taylor approximation that reduces guidance evaluations to a forward and backward pass. TESS2 (Tae et al. 2025) instead applies gradient ascent on a reward with respect to the model logits during inference to improve response quality. Finally, the Energy-based Diffusion Language Model (Xu et al. 2025) defines an energy over predicted clean sequences and uses it to importance-weight the denoising step, reducing the train-sample mismatch in discrete diffusion models.

Transfer Learning Fine-tuning and transfer learning share the goal of adapting a model to a new task or domain. Fine-tuning is computationally expensive because it updates the pretrained denoiser’s weights on new data. Prior work on continuous diffusion models explores reinforcement learning (Fan et al. 2023; Clark et al. 2024) and adapter-based fine-tuning (Moon et al. 2022; Xie et al. 2023). In contrast, transfer learning for diffusion remains comparatively underexplored. *Transfer Learning for Diffusion Models* (TLDM) proposes a ratio-estimation technique for continuous score-based models, but demonstrates effectiveness on synthetic data and a one-dimensional heartbeat dataset, leaving applications to higher-dimensional and large-scale domains open.

3 Background

Diffusion models are generative models defined by a forward noising process and a learned reverse denoising process. In the reverse process, a denoiser p_θ is trained to remove noise from latent variables \mathbf{z}_t to recover data x . The forward process generates \mathbf{z}_t by injecting noise into clean data. We consider discrete latents: $\mathbf{z}_t \in \mathcal{V}$, the set of one-hot tokens over a vocabulary of size N , $\mathcal{V} := \{\mathbf{z} \in \{0, 1\}^N : \sum_{i=1}^N z_i = 1\} \subset \Delta^{N-1}$, where Δ^{N-1} denotes the probability simplex over N categories. Let $\text{Cat}(\cdot; \pi)$ be the categor-

ical distribution over N classes with the probability vector $\pi \in \Delta^{N-1}$.

Discrete diffusion Discrete Denoising Diffusion Probabilistic Models (D3PMs) (Austin et al. 2023) provide a flexible framework for diffusion over discrete state spaces. The forward Markov chain is $p(\mathbf{z}_t | \mathbf{z}_s) = \text{Cat}(\mathbf{z}_t; Q_{t|s}\mathbf{z}_s)$ where $Q_{t|s} \in \mathbb{R}^{N \times N}$ is a transition matrix whose (i, j) entry is the probability of moving to state i at time t from state j at time s . To fit the generative model p_θ to the data distribution over \mathbf{x}_0 , we minimize the negative ELBO (NELBO). Different choices of $Q_{t|s}$ induce different corruption behaviors, e.g., uniform, absorbing, or discretized-Gaussian transitions.

Masked (absorbing-state) diffusion. The absorbing-state variant or often called *masked diffusion*, replaces tokens with a special [MASK] token (Sahoo et al. 2024; Shi et al. 2025). It can be viewed as an interpolation between the clean distribution and a noise prior over the vocabulary. For a clean token \mathbf{x}_0 , the forward transition at time t is

$$p(\mathbf{z}_t | \mathbf{x}_0) = \text{Cat}(\mathbf{z}_t; \alpha_t \mathbf{x}_0 + (1 - \alpha_t) \mathbf{m}), \quad (1)$$

where $\alpha_t \in [0, 1]$ controls the corruption schedule and $\mathbf{m} \in \mathcal{V}$ is one-hot vector at the special [MASK] token. Making use of the masking process, the backward posterior simplifies to:

$$p(\mathbf{z}_s | \mathbf{z}_t, \mathbf{x}_0) = \begin{cases} \text{Cat}(\mathbf{z}_s; \mathbf{z}_t), & \text{if } \mathbf{z}_t \neq \mathbf{m}, \\ \text{Cat}\left(\mathbf{z}_s; \frac{(1 - \alpha_s)\mathbf{m} + (\alpha_s - \alpha_t)\mathbf{x}_0}{1 - \alpha_t}\right), & \text{if } \mathbf{z}_t = \mathbf{m}. \end{cases} \quad (2)$$

Hence, when a token is unmasked ($\mathbf{x}_t \neq \mathbf{m}$) the step is deterministic: $\mathbf{x}_s = \mathbf{x}_t$. Otherwise, the posterior is a linear interpolation between the mask distribution and the clean token. This structure yields the simplified diffusion loss (Sahoo et al. 2024; Shi et al. 2025):

$$\mathcal{L}_{\text{diffusion}} = \sum_{i=1}^T D_{\text{KL}}(p(\mathbf{z}_{s(i)} | \mathbf{z}_{t(i)}, \mathbf{x}_0) \| p_\theta(\mathbf{z}_{s(i)} | \mathbf{z}_{t(i)})) \quad (3)$$

$$= \sum_{i=1}^T \mathbb{E}_q \left[\frac{\alpha_{t(i)} - \alpha_{s(i)}}{1 - \alpha_{t(i)}} \log \langle \mathbf{x}_\theta(\mathbf{z}_{t(i)}), \mathbf{x}_0 \rangle \right], \quad (4)$$

where \mathbf{x} is the one-hot encoding of the clean data and $\langle \cdot, \cdot \rangle$ is the inner product. The network \mathbf{x}_θ predicts the clean token distribution from the noisy input $\mathbf{z}_{t(i)}$.

Guidance Diffusion models provide strong controllability through both classifier-based and classifier-free guidance. These two approaches correspond to different ways of expressing the backward generative process conditioned on y . In this work, we focus on the classifier-based variant, which allows us to rearrange the conditional generative process using Bayes' rule as $p^\gamma(\mathbf{z}_s | \mathbf{z}_t, y) = p(y | \mathbf{z}_s, \mathbf{z}_t)^\gamma p(\mathbf{z}_s | \mathbf{z}_t) / Z$, with Z being a normalizing constant.

For the extension to sequences of tokens $\mathbf{z}_s^{(1:L)}$ of length L , we assume that the distribution $p^\gamma(\mathbf{z}_s^{(1:L)} | \mathbf{z}_t^{(1:L)}, y)$ factorizes independently across tokens. This leads to the following formulation:

$$p^\gamma(\mathbf{z}_s^{(1:L)} | \mathbf{z}_t^{(1:L)}, y) = \prod_{\ell=1}^L \frac{p(y | \mathbf{z}_s^{(\ell)}, \mathbf{z}_t^{(1:L)})^\gamma p(\mathbf{z}_s^{(\ell)} | \mathbf{z}_t^{(1:L)})}{\sum_{\tilde{\mathbf{z}}_s^{(\ell)} \in \mathcal{V}} p(y | \tilde{\mathbf{z}}_s^{(\ell)}, \mathbf{z}_t^{(1:L)})^\gamma p(\tilde{\mathbf{z}}_s^{(\ell)} | \mathbf{z}_t^{(1:L)})} \quad (5)$$

Here, \mathcal{V} denotes the vocabulary set, and $p(y | \mathbf{z}_s^{(\ell)}, \mathbf{z}_t^{(1:L)})$ represents the classifier probability given the sequence $\mathbf{z}_t^{(1:L)}$ with the token \mathbf{z}_s placed at position ℓ . However, this formulation comes with the drawback of requiring $\mathcal{O}(L \cdot |\mathcal{V}|)$ forward passes through the classifier model.

Problem Formulation Let \mathcal{X} denote the data space, with source domain distribution p_X and target domain distribution q_X . We are given source samples $\mathcal{S} = \{\mathbf{x}_i^{(1:L)}\}_{i=1}^m \sim p_X$ and target samples $\mathcal{T} = \{\mathbf{x}_i^{(1:L)}\}_{i=1}^n \sim q_X$. The goal of transfer learning is to train a network p_θ on \mathcal{S} and adapt it to \mathcal{T} to improve performance in the target domain. In practice, $n \ll m$, creating an imbalance between source and target data. A common strategy is to freeze most pretrained layers, extract features, and train new task-specific layers on \mathcal{T} . Fine-tuning relaxes this by unfreezing parameters, allowing the model to adapt more flexibly to the target distribution. In our setting, we are given a pretrained generative model p_θ trained on the source distribution p_X , and we aim to transfer its generative process to the target distribution q_X , yielding a target-domain model q_ψ . Note that the background section is introduced for the source domain diffusion.

4 Guided Transfer Learning for DDMs

We propose *Guided Transfer Learning for Discrete Diffusion Models*, a framework that enables transfer learning for discrete diffusion models. We first formalize the problem setup, then present the mathematical formulation of our method, and finally introduce a new sampling algorithm that leverages our results to make transfer learning broadly applicable across datasets.

Given the problem statement and access to both domains, one could fine-tune the source network p_θ by maximizing (4), thereby optimizing the entire parameter set. For large language models, this is often costly and slow due to the scale of parameters. Moreover, when the target domain provides far fewer samples, fine-tuning alone rarely yields a strong generative model in terms of diversity and quality.

Our method is based on the following theorem, which proposes a different approach to this problem: it leverages a pretrained source-domain diffusion model together with a ratio estimator between the two domains. We assume the two diffusion models share the same forward process $p(\mathbf{z}_t | \mathbf{x}_0) = q(\mathbf{z}_t | \mathbf{x}_0)$ for all t , that the density ratio $q(\mathbf{x}_0)/p(\mathbf{x}_0)$ is well defined.

Relation to TLDM. TLDM (Ouyang et al. 2024) proves a transfer result for continuous, score-based diffusion and is not directly applicable to discrete state spaces. The theorem is stated in \mathbb{R}^d and relies on score matching with differentiable densities, requiring gradients such as $\nabla_{x_t} \log q_t(x_t)$. In the discrete setting (categorical tokens), such Euclidean scores are undefined. Beyond this, the modeling and training objectives differ: continuous diffusion injects Gaussian noise and optimizes score-matching Mean Squared Error, whereas discrete diffusion uses categorical transition matrices (e.g., absorbing/uniform) and is trained by minimizing KL between categorical true posteriors $q(\mathbf{z}_s \mid \mathbf{z}_t, \mathbf{x}_0)$ and $q_\psi(\mathbf{z}_s \mid \mathbf{z}_t)$.

Theorem 1 *Let p (source) and q (target) be two diffusion models that share the same forward process, $p(\mathbf{z}_t \mid \mathbf{x}_0) = q(\mathbf{z}_t \mid \mathbf{x}_0)$ for all t . The reverse target domain network $q_\theta(\mathbf{z}_{s(i)} \mid \mathbf{z}_{t(i)})$ is defined by:*

$$\arg \min_{\psi} \mathbb{E}_q \left[\sum_{i=1}^T D_{\text{KL}} \left(q(\mathbf{z}_{s(i)} \mid \mathbf{z}_{t(i)}, \mathbf{x}_0) \parallel q_\psi(\mathbf{z}_{s(i)} \mid \mathbf{z}_{t(i)}) \right) \right] \quad (6)$$

Then we have

$$q_{\psi^*}(\mathbf{z}_{s(i)} \mid \mathbf{z}_{t(i)}) = \frac{p(\mathbf{z}_{s(i)} \mid \mathbf{z}_{t(i)}) \mathbb{E}_{\mathbf{x}_0 \sim p(\cdot \mid \mathbf{z}_{s(i)})} \left[\frac{q(\mathbf{x}_0)}{p(\mathbf{x}_0)} \right]}{\sum_{\tilde{\mathbf{z}}_{s(i)}} p(\tilde{\mathbf{z}}_{s(i)} \mid \mathbf{z}_{t(i)}) \mathbb{E}_{\mathbf{x}_0 \sim p(\cdot \mid \tilde{\mathbf{z}}_{s(i)})} \left[\frac{q(\mathbf{x}_0)}{p(\mathbf{x}_0)} \right]} \quad (7)$$

In (7), $p(\mathbf{z}_{s(i)} \mid \mathbf{z}_{t(i)}) \approx p_\theta(\mathbf{z}_{s(i)} \mid \mathbf{z}_{t(i)})$ is the trained denoiser on the source domain, and the expectation factor $r_\phi(\mathbf{z}_{s(i)}) \approx \mathbb{E}_{\mathbf{x}_0 \sim p(\cdot \mid \mathbf{z}_{s(i)})} \left[\frac{q(\mathbf{x}_0)}{p(\mathbf{x}_0)} \right]$ is the guidance ratio. Thus, the target diffusion process can be approximated with two networks $\psi^* = [\theta, \phi]$. The proof of this theorem can be found in the supplementary materials. The advantage of this approach is that it does not require fine-tuning the pre-trained discrete diffusion model. Instead, the main computational cost is shifted to training a domain classifier using both domains as data. Importantly, the domain classifier can be much smaller than the discrete diffusion model. Moreover, density ratio estimation provides more flexibility in regularization when dealing with highly imbalanced data. It only requires distinguishing domains rather than modeling the full target distribution, which makes the training dynamics between the discriminative and generative models more stable.

The result in (Ouyang et al. 2024) is derived only for score-based diffusion in continuous data domains. But our formulation in (7) offers two advantages: (i) it permits flexible definitions of the forward and reverse discrete diffusion processes, and (ii) the guidance term can be trained under arbitrary noise processes, in either continuous- or discrete-time settings.

In the supplementary materials (Theorem 3), we extend the result to the score-based, continuous-time diffusion setting over discrete state spaces. The key mathematical step is to trace back through to the ELBO formulation used in (6). For the masked (absorbing-state) diffusion training objective, this link is directly shown in Equation (4).

Method	Per-Step Complexity	Number of Steps (T)
Ancestral Sampling	$\mathcal{O}(\mathcal{V} \cdot L)$	T
+ Caching	$\mathcal{O}(\mathcal{V} \cdot L)$	$T' \leq \min(L, T)$
+ Top- n_{ratio}	$\mathcal{O}(n_{\text{ratio}} \cdot L)$	$T' \leq \min(L, T)$
Planner Sampling		
+ Top- n_{ratio}	$\mathcal{O}(n_{\text{ratio}})$	L

Table 1: Computational cost per denoising step and total number of steps.

Extension to Sequence Leveraging our theoretical results, (7) closely parallels (5). Instead of a classifier $p(y \mid \mathbf{z}_s^{(\ell)}, \mathbf{z}_t^{(1:L)})$, we use a ratio network $r_\phi(\mathbf{z}_{s(i)}) \approx \mathbb{E}_{\mathbf{x}_0 \sim p(\cdot \mid \mathbf{z}_{s(i)})} \left[\frac{q(\mathbf{x}_0)}{p(\mathbf{x}_0)} \right]$. To extend this to sequences, define $\mathbf{z}_{t,s^\ell}^{(1:L)} := [\mathbf{z}_t^{(1:\ell-1)}, \mathbf{z}_s^{(\ell)}, \mathbf{z}_t^{(\ell+1:L)}]$, i.e., the sequence identical to $\mathbf{z}_t^{(1:L)}$ except at position ℓ , where the token is replaced by $\mathbf{z}_s^{(\ell)}$. This yields the following factorized, ratio-guided conditional (with guidance strength $\gamma \geq 0$):

$$q_{\theta, \phi}(\mathbf{z}_s^{(1:L)} \mid \mathbf{z}_t^{(1:L)}) = \prod_{\ell=1}^L \frac{[r_\phi(\mathbf{z}_{t,s^\ell}^{(1:L)})]^\gamma p_\theta(\mathbf{z}_s^{(\ell)} \mid \mathbf{z}_t^{(1:L)})}{\sum_{\tilde{\mathbf{z}}_s^{(\ell)} \in \mathcal{V}} [r_\phi(\mathbf{z}_{t,\tilde{s}^\ell}^{(1:L)})]^\gamma p_\theta(\tilde{\mathbf{z}}_s^{(\ell)} \mid \mathbf{z}_t^{(1:L)})} \quad (8)$$

A naive integration of this guidance into the sampling process incurs a computational complexity of $\mathcal{O}(|\mathcal{V}| \cdot L)$ per denoising step, since we must evaluate r_ϕ for all sequences obtained by replacing every possible token in \mathcal{V} at each position L in the denominator. Prior work (Schiff et al. 2025; Nisonoff et al. 2025) targets settings with modest vocabulary sizes and sequence lengths, where this cost is manageable. In our experiments with the Markov chain (Section 5.1) it is also not prohibitive. But for text applications, the cost becomes significant. (Nisonoff et al. 2025) proposes a first-order Taylor approximation that reduces evaluations, but it is accurate primarily in the high-noise regime and degrades as t decreases.

4.1 Scalability via Planner Sampling

In this section, we tackle the main bottleneck: integrating guidance efficiently at inference time. The gains from a set of simple techniques are summarized in Table 1.

Ancestral Sampling In the naive implementation, at all denoising steps, we compute logits from the denoiser and from the guidance network with $\mathcal{O}(|\mathcal{V}| \cdot L)$ complexity. Following (Sahoo et al. 2024), in masked diffusion, we can remove explicit time conditioning because the number of masked tokens in the sequence already implies the timestep. This is not possible for uniform noise, which mixes token identities. We therefore cache logits across steps. If a step does not change the sequence, we reuse the logits from the previous step. The number of sampling steps where the network is called then becomes upper-bounded by the sequence

Algorithm 1: Ratio-Guided Denoise Step ($\mathbf{z}_t, t, \Delta t$).

Require: noisy sequence $\mathbf{z}_t \in \mathcal{V}^L$, denoiser p_θ , ratio net r_ϕ , guidance schedule $\gamma(\cdot)$, planner ρ_θ

- 1: $\ell \leftarrow \rho_\theta(\mathbf{z}_t)$ {Get position by planner}
- 2: $\log x_\theta \leftarrow p_\theta(\mathbf{z}_t)$
- 3: $\mathcal{N} \leftarrow$ Top N tokens in $\log x_\theta[\ell, :]$
- 4: **for all** $v \in \mathcal{N}$ **do**
- 5: $\tilde{\mathbf{z}} \leftarrow (\mathbf{z}_t[\ell] \leftarrow v)$
- 6: $\log r[\ell, v] \leftarrow r_\phi(\tilde{\mathbf{z}}, \sigma_t)$ {Ratio scores}
- 7: **end for**
- 8: $\log q^{\text{guided}}[\ell, :] \leftarrow \log x_\theta[\ell, :] + \gamma(t) \log r[\ell, :]$
- 9: $\log q^{\text{guided}}[\ell, \mathcal{V} \setminus \mathcal{N}] \leftarrow -\infty$ {set non-Top- N tokens $-\infty$ }
- 10: $\pi \leftarrow \text{softmax}(\log q^{\text{guided}}[\ell, :])$
- 11: $\mathbf{z}_t^{(\ell)} \sim \text{Cat}(\pi[\ell, :])$ {Sample at ℓ }
- 12: $\mathbf{z}_s \leftarrow \mathbf{z}_t$
- 13: **return** \mathbf{z}_s

length, since in the worst case, every position unmasks in a different step.

In addition, we introduce a top- n style pruning mechanism for the ratio network. Specifically, we assume that (i) the denoiser distribution $p_\theta(\cdot | z_t)$ is sufficiently concentrated, so that the true target distribution q differs from p only within the top- n_{ratio} candidates, and (ii) the density ratio $r(z) = q(z)/p(z)$ is bounded, in the sense that there exists a constant $C < \infty$ such that for all tokens within the top- n_{ratio} set of p_θ , we have $\frac{q(z)}{p(z)} \leq C$. Outside this set, where $p(z)$ is already very small, no such bound is required. Consequently, we evaluate the ratio term only for the top n_{ratio} candidates proposed by the denoiser at each position. This results in position-specific candidate sets in the denominator of equation (8) and reduces the computational cost of ratio evaluations to $\mathcal{O}(n_{\text{ratio}} \cdot L)$ with $n_{\text{ratio}} \leq |\mathcal{V}|$. In the experiments, the combination of top- n_{ratio} selection and the guidance weight γ can misallocate probability mass, which may cause the diffusion process to collapse into a fully masked sequence at the final step. Thus, a key assumption is that the probability of remaining a masked token must be equal between the target and source distributions. As a result, we enforce a position-independent normalization which implies the renormalized update over non-mask tokens, thus stabilizing the denoising diffusion process. Further details of this stabilizer are presented in the supplementary materials.

Planner Sampling We also apply our method to text in Section 5.2, where $n_{\text{ratio}} \ll |\mathcal{V}|$, yet sampling remains slow and costly mainly because of the L in the complexity. To address this, we propose a *planner-based algorithm*. The planner ρ_θ is trained to predict the next denoising position in the masked sequence. Concretely, we replace the Gillespie process with τ -leaping by a planner schedule that unmasks exactly one position per step, thereby fixing the number of denoising steps to L . In many implementations, $T \approx L$, so enforcing a hard budget of L steps does not materially change the step count, while reducing guidance evaluations and wall-clock time. Pseudocode is provided in Algorithm 1.

An important achievement here is that the loop in lines 4 to 7 can now be parallelized by vectorization on a single GPU. As a result, only one forward pass of the three networks is required.

For training the planner, we adopt a simplified training algorithm following (Peng et al. 2025; Liu et al. 2025). For ratio training, we use a discrete data training loss function building on the work of (Ouyang et al. 2024). Further details of the loss function and training algorithm are provided in the supplementary materials.

5 Experiments

In this section, we present empirical results on the effectiveness of our method, Guided Transfer Learning for discrete diffusion models (GTL). We provide evidence across two applications showing that our method can successfully sample from the target distribution, in comparison to a vanilla diffusion model and standard finetuning. The first section presents a proof-of-concept on a synthetic dataset based on learning Markov chain data. The second subsection reports results on language modeling using arXiv abstracts.

5.1 Synthetic Dataset

Experimental Setup We construct two Markov chains with distinct transition matrices. Let the probability state vector be $\pi_i \in \Delta^{N-1}$ over a vocabulary of size $N = 5$. The transition matrix of the target domain is $\mathbf{T} \in \mathbb{R}^{N \times N}$ and that of the source domain is $\mathbf{S} \in \mathbb{R}^{N \times N}$. We sample sequences of length 20 from the target domain using the update rule $\pi_i = \mathbf{T} \pi_{i-1}$ with the initial state π_0 set to the uniform vector. Sampling from the source domain proceeds in the same way.

Implementation We use the sampling process of (Sahoo et al. 2024) for the source, finetuned, and target discrete diffusion models. The backbone is a Diffusion Transformer (DiT) (Peebles and Xie 2023) with about five million learnable parameters. The ratio estimator and the classifier use about half as many parameters with a final mean and fully connected layer that maps the output to a scalar. The exact implementation appears in our codebase. For guided sampling, we follow the ancestral sampling method. Since the vocabulary is small we set $n_{\text{ratio}} = N$ and use 20 sampling steps. We train a masked diffusion model on the source domain for 30 epochs. We then compare a vanilla masked diffusion model trained directly on the target samples (60 epochs), a finetuned diffusion model (90 epochs), and our GTL method (60 epochs). The finetuned model and our method share the same source diffusion model.

Results We consider $m = 10000$ source samples and $n \in \{1000, 100, 20\}$ target samples. We estimate the transition matrix by sampling 4096 sequences, counting transitions between states, and normalizing by the total count. Figure 2 presents an example where \mathbf{S} has diagonal entries 0.1 and \mathbf{T} has diagonal entries 0.8. We observe that the vanilla target diffusion model and the finetuned model both degrade in performance when fewer target samples are available. Table 2 provides a direct comparison, obtained by running this

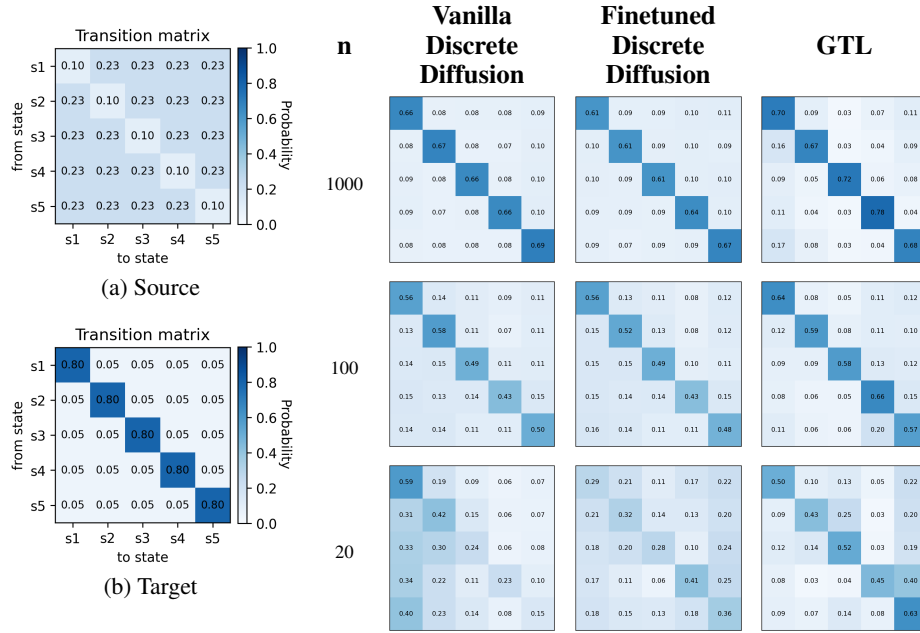


Figure 2: True source and target (left). Estimated target transition matrices for varying n across three methods (right).

n_{tgt}	Vanilla (Target-only)	Finetuned	GTL
1000	0.0476 ± 0.0064	0.0393 ± 0.0029	0.0377 ± 0.0080
100	0.1938 ± 0.0173	0.1118 ± 0.0271	0.0989 ± 0.0180
20	0.5842 ± 0.0244	0.4004 ± 0.0983	0.3621 ± 0.0478

Table 2: Comparison of baseline methods and best guided results (mean \pm standard error; $n=3$ seeds) across target sample sizes for ($\text{diag}_{\text{src}} = 0.1, \text{diag}_{\text{tgt}} = 0.8$). Reported values are the average Kullback–Leibler divergence between true and estimated transition matrices; lower is better.

example three times with different random seeds. We observe the following behaviors: (i) the diffusion model trained directly on the target dataset loses performance as the number of training samples decreases, and (ii) our method, compared to traditional finetuning, achieves better results even with fewer trainable parameters, while showing a similar trend in performance across different numbers of training samples.

5.2 Language Modeling

In this section, we apply our method to text data. We use the arXiv abstracts dataset (arXiv.org submitters 2024), which contains 1.7 million arXiv articles with titles, authors, categories, and abstracts. We focus on Computer Science, Mathematics, and Physics. For data preparation, we concatenate all text and split it into segments of 512 tokens using the `bert-base-uncased` tokenizer with vocabulary size $N = 30,522$. This results in 285,946 samples in Computer Science, 176,831 in Mathematics, and 79,631 in Physics. For each category we randomly select 10% of the samples for validation. We ensure that the three category subsets

are disjoint. We define the union of Computer Science and Mathematics as the source domain and Physics as the target domain.

We run two types of experiments. First, we study the behavior of the two key parameters γ and n_{ratio} . Second, we compare three settings on the target domain. The first is a vanilla discrete diffusion model trained on the target data. The second is a finetuned version of the source model. The third is our guided transfer method.

Implementation and Evaluations We train the source diffusion model for 100,000 gradient steps using the DiT architecture (Peebles and Xie 2023) with 59.8M trainable parameters. A log–linear noise scheduler is used for both training and sampling. The finetuned model on the target domain is trained for 10,000 gradient steps. For our guided method, we initialize a ratio model with 4.1M parameters and train it for 5,000 gradient steps. Additional training details appear in the supplementary materials.

For each method we generate 128 sequences of length 512. We evaluate quality with MAUVE (Pillutla et al. 2021), which captures the tradeoff between perplexity and diversity. Although generative perplexity (Gen. PPL) is often reported, we observed, consistent with prior work (Wang et al. 2025), that Gen. PPL can remain low even when the text has reduced utility, such as repeated words. In those cases, MAUVE is more sensitive and provides a clearer measure of quality. We also evaluate the domain of each sampled sequence using an independently trained classifier. Scores near zero indicate the target domain and scores near one indicate the source domain. The classifier follows the setup used for the ratio model in the supplementary materials with label smoothing set to 0.05.

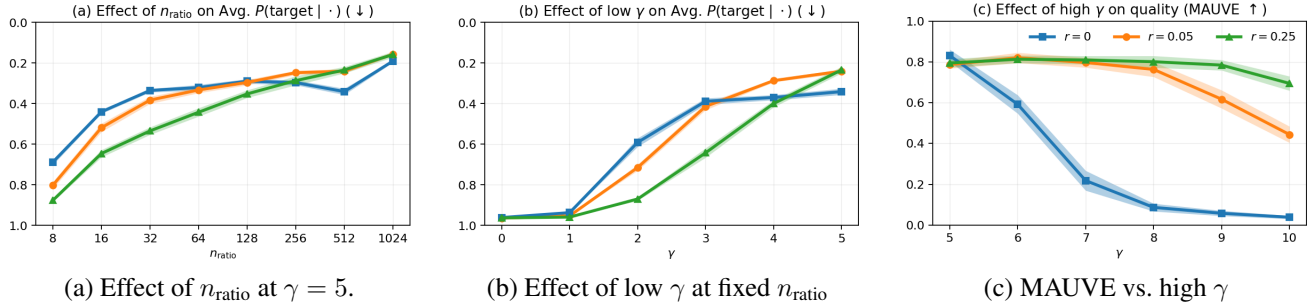


Figure 3: Sensitivity of GTL to the guidance weight γ and the candidate budget n_{ratio} on Physics (validation). For each setting we train three independent source models and three ratio models (different seeds). The source domain is $\mathcal{S} = \text{CS} \cup \text{Math} \cup \mathcal{P}_r$ and the target domain is $\mathcal{T} = \mathcal{P} \setminus \mathcal{P}_r$, where \mathcal{P}_r is a random r -subset of Physics (sampled without replacement). Lines show means; shaded bands are $\pm \text{SE}$ over 3×3 train \times sample seeds. Legend values of r indicate the fraction of Physics included in the source.

Behavior of γ and n_{ratio} We study the sensitivity of GTL to the guidance weight γ and the candidate budget n_{ratio} . For each configuration, we train three independent source models and three ratio models using different random seeds. The source domain is defined as Computer Science \cup Mathematics plus an r -fraction of Physics abstracts, and the target domain is the remaining $(1 - r)$ fraction of Physics. Formally, for $r \in [0, 1]$, let \mathcal{P}_r be a random r -subset of Physics (sampled without replacement). We set $\mathcal{S} = \text{CS} \cup \text{Math} \cup \mathcal{P}_r$ and $\mathcal{T} = \mathcal{P} \setminus \mathcal{P}_r$. We set $r \in \{0, 0.05, 0.25\}$, thus in the case of $r = 0$ we have two distinct datasets. This setup simulates the common scenario where pretraining large corpora already includes a small portion of target-domain text. In Figure 3, the behavior of these parameters is illustrated. Intuitively, smaller candidate budgets n_{ratio} introduce higher sampling error, whereas increasing n_{ratio} monotonically reduces the domain-classifier score, yielding more target-like samples, as shown in panel (a). In Figure 3(b), we observe that the guidance score is nontrivial: a moderate $\gamma \approx 3 - 5$ consistently pushes the representations toward the target across all r . Panel (c) highlights two key effects: (i) excessive guidance can degrade performance when there is no overlap between source and target data, and (ii) when a small portion of target text is included in the source domain ($r = 0.05, 0.25$), MAUVE remains high for larger γ values and decays more smoothly. This indicates that a higher r improves robustness. Overall, the results suggest that $n_{\text{ratio}} \approx 256 - 512$ and $\gamma \approx 4 - 6$ achieve a favorable balance, providing strong target alignment with minimal quality loss.

Method Comparison and Sensitivity to Data Fraction

We compare three methods: a fine-tuned discrete diffusion model trained on the target domain after pretraining on the source domain, a vanilla discrete diffusion model trained directly on the target domain, and our Guided Transfer Learning (GTL) method with the ratio estimator trained across target-data fractions of 100%, 30%, 5%, and 1%. Each method is trained with three random seeds, and sampling is performed with three seeds as well (nine runs per cell). Furthermore, each seed corresponds to a distinct subset of the target data. Figure 1 reports the behavior of the mod-

els across different fractions of the target training data. The observed trends align with those in Table 2. In the smallest case, we only use 796 samples of Physics abstracts. For fine-tuned and vanilla discrete diffusion, the number of epochs over the training set increases up to 400 when the fraction is smallest. The ratio model decreases its MAUVE score with decreasing fractions, but less dramatically than the other methods. Thus, our method demonstrates greater stability under limited target-domain data. In contrast, the finetuned and vanilla discrete diffusion models show a stepwise drop in performance as the fraction decreases. The GTL remains relatively stable, except in the 1% case, where we also observe a sharp decline.

6 Conclusion

Adapting discrete diffusion models to target domains with limited data is often costly. To address this, we propose a guided transfer learning approach for discrete diffusion models that introduces a small, learned ratio network, allowing the training of significantly fewer parameters. Furthermore, we present a guidance-based sampling algorithm that enables generation with larger vocabularies and longer sequences, making guided language modeling with discrete diffusion models feasible. We demonstrate the effectiveness of our method on synthetic Markov chains and arXiv abstracts (language modeling), particularly when the target dataset is small relative to the source.

Limitations Overall, the proposed method is promising and applicable to a wide range of tasks involving domain shifts. However, it requires access to both source and target domains. Future work could explore conditional transfer for prompt-based or attribute-controlled generation. It would also be interesting to evaluate the learned ratio on quality-filtered tasks, such as reducing toxicity in language modeling.

References

arXiv.org submitters. 2024. arXiv Dataset.

- Austin, J.; Johnson, D. D.; Ho, J.; Tarlow, D.; and van den Berg, R. 2023. Structured Denoising Diffusion Models in Discrete State-Spaces. *arXiv:2107.03006*.
- Campbell, A.; Benton, J.; Bortoli, V. D.; Rainforth, T.; Deligiannidis, G.; and Doucet, A. 2022. A Continuous Time Framework for Discrete Denoising Models. *arXiv:2205.14987*.
- Clark, K.; Vicol, P.; Swersky, K.; and Fleet, D. J. 2024. Directly Fine-Tuning Diffusion Models on Differentiable Rewards. *arXiv:2309.17400*.
- Fan, Y.; Watkins, O.; Du, Y.; Liu, H.; Ryu, M.; Boutilier, C.; Abbeel, P.; Ghavamzadeh, M.; Lee, K.; and Lee, K. 2023. DPOK: Reinforcement Learning for Fine-tuning Text-to-Image Diffusion Models. *arXiv:2305.16381*.
- Gong, S.; Agarwal, S.; Zhang, Y.; Ye, J.; Zheng, L.; Li, M.; An, C.; Zhao, P.; Bi, W.; Han, J.; Peng, H.; and Kong, L. 2025. Scaling Diffusion Language Models via Adaptation from Autoregressive Models. *arXiv:2410.17891*.
- Ho, J.; Jain, A.; and Abbeel, P. 2020. Denoising Diffusion Probabilistic Models. *arXiv:2006.11239*.
- Ho, J.; Salimans, T.; Gritsenko, A.; Chan, W.; Norouzi, M.; and Fleet, D. J. 2022. Video Diffusion Models. *arXiv:2204.03458*.
- Huang, C.; and Tang, H. 2025. CtrlDiff: Boosting Large Diffusion Language Models with Dynamic Block Prediction and Controllable Generation. *arXiv:2505.14455*.
- Li, X. L.; Thickstun, J.; Gulrajani, I.; Liang, P.; and Hashimoto, T. B. 2022a. Diffusion-LM Improves Controllable Text Generation. *arXiv:2205.14217*.
- Li, X. L.; Thickstun, J.; Gulrajani, I.; Liang, P.; and Hashimoto, T. B. 2022b. Diffusion-LM Improves Controllable Text Generation. *arXiv:2205.14217*.
- Liu, H.; Chen, Z.; Yuan, Y.; Mei, X.; Liu, X.; Mandic, D.; Wang, W.; and Plumbley, M. D. 2023. AudioLDM: Text-to-Audio Generation with Latent Diffusion Models. *arXiv:2301.12503*.
- Liu, S.; Nam, J.; Campbell, A.; Stärk, H.; Xu, Y.; Jaakkola, T.; and Gómez-Bombarelli, R. 2025. Think While You Generate: Discrete Diffusion with Planned Denoising. *arXiv:2410.06264*.
- Lou, A.; Meng, C.; and Ermon, S. 2024. Discrete Diffusion Modeling by Estimating the Ratios of the Data Distribution. *arXiv:2310.16834*.
- Lovelace, J.; Kishore, V.; Wan, C.; Shekhtman, E.; and Weinberger, K. Q. 2023. Latent Diffusion for Language Generation. *arXiv:2212.09462*.
- Meng, C.; Choi, K.; Song, J.; and Ermon, S. 2023. Concrete Score Matching: Generalized Score Matching for Discrete Data. *arXiv:2211.00802*.
- Moon, T.; Choi, M.; Lee, G.; Ha, J.-W.; and Lee, J. 2022. Fine-tuning Diffusion Models with Limited Data. In *NeurIPS 2022 Workshop on Score-Based Methods*.
- Nie, S.; Zhu, F.; Du, C.; Pang, T.; Liu, Q.; Zeng, G.; Lin, M.; and Li, C. 2025. Scaling up Masked Diffusion Models on Text. *arXiv:2410.18514*.
- Nisonoff, H.; Xiong, J.; Allenspach, S.; and Listgarten, J. 2025. Unlocking Guidance for Discrete State-Space Diffusion and Flow Models. *arXiv:2406.01572*.
- Ouyang, Y.; Xie, L.; Zha, H.; and Cheng, G. 2024. Transfer Learning for Diffusion Models. *arXiv:2405.16876*.
- Peebles, W.; and Xie, S. 2023. Scalable Diffusion Models with Transformers. *arXiv:2212.09748*.
- Peng, F. Z.; Bezemek, Z.; Patel, S.; Rector-Brooks, J.; Yao, S.; Bose, A. J.; Tong, A.; and Chatterjee, P. 2025. Path Planning for Masked Diffusion Model Sampling. *arXiv:2502.03540*.
- Pillutla, K.; Swayamdipta, S.; Zellers, R.; Thickstun, J.; Welleck, S.; Choi, Y.; and Harchaoui, Z. 2021. MAUVE: Measuring the Gap Between Neural Text and Human Text using Divergence Frontiers. *arXiv:2102.01454*.
- Sahoo, S. S.; Arriola, M.; Schiff, Y.; Gokaslan, A.; Marroquin, E.; Chiu, J. T.; Rush, A.; and Kuleshov, V. 2024. Simple and Effective Masked Diffusion Language Models. *arXiv:2406.07524*.
- Sarkar, A.; Tang, Z.; Zhao, C.; and Koo, P. K. 2024. Designing DNA With Tunable Regulatory Activity Using Discrete Diffusion. *bioRxiv*.
- Schiff, Y.; Sahoo, S. S.; Phung, H.; Wang, G.; Boshar, S.; Dalla-torre, H.; de Almeida, B. P.; Rush, A.; Pierrot, T.; and Kuleshov, V. 2025. Simple Guidance Mechanisms for Discrete Diffusion Models. *arXiv:2412.10193*.
- Shi, J.; Han, K.; Wang, Z.; Doucet, A.; and Titsias, M. K. 2025. Simplified and Generalized Masked Diffusion for Discrete Data. *arXiv:2406.04329*.
- Song, Y.; Sohl-Dickstein, J.; Kingma, D. P.; Kumar, A.; Ermon, S.; and Poole, B. 2021. Score-Based Generative Modeling through Stochastic Differential Equations. *arXiv:2011.13456*.
- Sun, H.; Yu, L.; Dai, B.; Schuurmans, D.; and Dai, H. 2023. Score-based Continuous-time Discrete Diffusion Models. *arXiv:2211.16750*.
- Tae, J.; Ivison, H.; Kumar, S.; and Cohan, A. 2025. TESS 2: A Large-Scale Generalist Diffusion Language Model. *arXiv:2502.13917*.
- Wang, G.; Schiff, Y.; Sahoo, S. S.; and Kuleshov, V. 2025. Remasking Discrete Diffusion Models with Inference-Time Scaling. *arXiv:2503.00307*.
- Xie, E.; Yao, L.; Shi, H.; Liu, Z.; Zhou, D.; Liu, Z.; Li, J.; and Li, Z. 2023. DiffFit: Unlocking Transferability of Large Diffusion Models via Simple Parameter-Efficient Fine-Tuning. *arXiv:2304.06648*.
- Xu, M.; Geffner, T.; Kreis, K.; Nie, W.; Xu, Y.; Leskovec, J.; Ermon, S.; and Vahdat, A. 2025. Energy-Based Diffusion Language Models for Text Generation. *arXiv:2410.21357*.
- Ye, J.; Gao, J.; Gong, S.; Zheng, L.; Jiang, X.; Li, Z.; and Kong, L. 2025. Beyond Autoregression: Discrete Diffusion for Complex Reasoning and Planning. *arXiv:2410.14157*.
- Yu, R.; Li, Q.; and Wang, X. 2025. Discrete Diffusion in Large Language and Multimodal Models: A Survey. *arXiv:2506.13759*.

Zheng, K.; Chen, Y.; Mao, H.; Liu, M.-Y.; Zhu, J.; and Zhang, Q. 2025. Masked Diffusion Models are Secretly Time-Agnostic Masked Models and Exploit Inaccurate Categorical Sampling. arXiv:2409.02908.

Zhong, J.; Zhang, X.; Wang, J.; and Long, M. 2025. Domain Guidance: A Simple Transfer Approach for a Pre-trained Diffusion Model. arXiv:2504.01521.

7 Supplementary Materials for Guided Transfer Learning for Discrete Diffusion Models

A Proof of Theorem 1

For the proof, we use the formulation of importance reweighting as described in the following lemma.

Lemma 2 (Importance-weighted reformulation) Fix a timestep i and define $r(\mathbf{x}_0) = q(\mathbf{x}_0)/p(\mathbf{x}_0)$. If the source and target share the same forward process, then the loss function can be rewritten as:

$$\mathcal{L}_i(\psi) = \mathbb{E}_q [D_{\text{KL}}(q(\mathbf{z}_{s(i)} | \mathbf{z}_{t(i)}, \mathbf{x}_0) \| q_\psi(\mathbf{z}_{s(i)} | \mathbf{z}_{t(i)}))] \quad (9)$$

$$= \mathbb{E}_{\mathbf{x}_0 \sim p} \mathbb{E}_{\mathbf{z}_{t(i)} \sim p(\mathbf{z}_{t(i)} | \mathbf{x}_0)} \left[r(\mathbf{x}_0) D_{\text{KL}}(p(\mathbf{z}_{s(i)} | \mathbf{z}_{t(i)}, \mathbf{x}_0) \| q_\psi(\mathbf{z}_{s(i)} | \mathbf{z}_{t(i)})) \right]. \quad (10)$$

Proof of Lemma 2

$$\mathbb{E}_q [\mathcal{L}_{\text{diffusion}}] = \sum_{i=1}^T \mathbb{E}_q [D_{\text{KL}}(q(\mathbf{z}_{s(i)} | \mathbf{z}_{t(i)}, \mathbf{x}_0) \| q_\psi(\mathbf{z}_{s(i)} | \mathbf{z}_{t(i)}))] \quad (11)$$

$$= \sum_{i=1}^T \sum_{\mathbf{x}_0} \sum_{\mathbf{z}_{t(i)}} q(\mathbf{x}_0, \mathbf{z}_{t(i)}) D_{\text{KL}}(q(\mathbf{z}_{s(i)} | \mathbf{z}_{t(i)}, \mathbf{x}_0) \| q_\psi(\mathbf{z}_{s(i)} | \mathbf{z}_{t(i)})) \quad (12)$$

$$= \sum_{i=1}^T \sum_{\mathbf{x}_0} \sum_{\mathbf{z}_{t(i)}} q(\mathbf{x}_0) q(\mathbf{z}_{t(i)} | \mathbf{x}_0) D_{\text{KL}}(q(\mathbf{z}_{s(i)} | \mathbf{z}_{t(i)}, \mathbf{x}_0) \| q_\psi(\mathbf{z}_{s(i)} | \mathbf{z}_{t(i)})) \quad (13)$$

$$= \sum_{i=1}^T \sum_{\mathbf{x}_0} \sum_{\mathbf{z}_{t(i)}} \frac{q(\mathbf{x}_0)}{p(\mathbf{x}_0)} p(\mathbf{x}_0) p(\mathbf{z}_{t(i)} | \mathbf{x}_0) D_{\text{KL}}(q(\mathbf{z}_{s(i)} | \mathbf{z}_{t(i)}, \mathbf{x}_0) \| q_\psi(\mathbf{z}_{s(i)} | \mathbf{z}_{t(i)})) \quad (14)$$

$$= \sum_{i=1}^T \mathbb{E}_{\mathbf{x}_0 \sim p} \mathbb{E}_{\mathbf{z}_{t(i)} \sim p(\mathbf{z}_{t(i)} | \mathbf{x}_0)} \left[\frac{q(\mathbf{x}_0)}{p(\mathbf{x}_0)} D_{\text{KL}}(p(\mathbf{z}_{s(i)} | \mathbf{z}_{t(i)}, \mathbf{x}_0) \| q_\psi(\mathbf{z}_{s(i)} | \mathbf{z}_{t(i)})) \right] \quad (15)$$

To conclude Lemma 2, we leverage the fact that the source and target domain share the same forward kernel in Equation 14 to 15 $q(\mathbf{z}_{s(i)} | \mathbf{z}_{t(i)}, \mathbf{x}_0) = \frac{q(\mathbf{z}_{t(i)} | \mathbf{z}_{s(i)}) \cdot q(\mathbf{z}_{s(i)} | \mathbf{x}_0)}{q(\mathbf{z}_{t(i)} | \mathbf{x}_0)} = p(\mathbf{z}_{s(i)} | \mathbf{z}_{t(i)}, \mathbf{x}_0)$.

Now, we use Lemma 2:

$$\mathcal{L}_i(\psi) = \mathbb{E}_{\mathbf{x}_0 \sim p} \mathbb{E}_{\mathbf{z}_{t(i)} \sim p(\mathbf{z}_{t(i)} | \mathbf{x}_0)} \left[\underbrace{\frac{q(\mathbf{x}_0)}{p(\mathbf{x}_0)}}_{r(\mathbf{x}_0)} D_{\text{KL}}(p(\mathbf{z}_{s(i)} | \mathbf{z}_{t(i)}, \mathbf{x}_0) \| q_\psi(\mathbf{z}_{s(i)} | \mathbf{z}_{t(i)})) \right] \quad (16)$$

$$= \sum_{\mathbf{x}_0} \sum_{\mathbf{z}_{t(i)}} \underbrace{p(\mathbf{z}_{t(i)} | \mathbf{x}_0) p(\mathbf{x}_0)}_{p(\mathbf{x}_0 | \mathbf{z}_{t(i)}) p(\mathbf{z}_{t(i)})} r(\mathbf{x}_0) D_{\text{KL}}(p(\mathbf{z}_{s(i)} | \mathbf{z}_{t(i)}, \mathbf{x}_0) \| q_\psi(\mathbf{z}_{s(i)} | \mathbf{z}_{t(i)})) \quad (17)$$

$$= \sum_{\mathbf{z}_{t(i)}} p(\mathbf{z}_{t(i)}) \sum_{\mathbf{x}_0} \underbrace{p(\mathbf{x}_0 | \mathbf{z}_{t(i)}) r(\mathbf{x}_0)}_{\alpha(\mathbf{x}_0, \mathbf{z}_{t(i)})} D_{\text{KL}}(p(\mathbf{z}_{s(i)} | \mathbf{z}_{t(i)}, \mathbf{x}_0) \| q_\psi(\mathbf{z}_{s(i)} | \mathbf{z}_{t(i)})) \quad (18)$$

$$= \sum_{\mathbf{z}_{t(i)}} p(\mathbf{z}_{t(i)}) \sum_{\mathbf{x}_0} \alpha(\mathbf{x}_0, \mathbf{z}_{t(i)}) D_{\text{KL}}(p(\mathbf{z}_{s(i)} | \mathbf{z}_{t(i)}, \mathbf{x}_0) \| q_\psi(\mathbf{z}_{s(i)} | \mathbf{z}_{t(i)})) \quad (19)$$

Now, we take the derivative in regard to ψ :

$$0 = \frac{\partial}{\partial \psi} \mathcal{L}_i(\psi) \quad (20)$$

$$\implies 0 = \frac{\partial}{\partial \psi} \sum_{\mathbf{x}_0} \alpha(\mathbf{x}_0, \mathbf{z}_{t(i)}) D_{\text{KL}}(p(\mathbf{z}_{s(i)} | \mathbf{z}_{t(i)}, \mathbf{x}_0) \| q_\psi(\mathbf{z}_{s(i)} | \mathbf{z}_{t(i)})) \quad (21)$$

To solve this, we set up a Lagrangian equation by using the constraint $\sum_{\mathbf{z}_{s(i)}} q_\psi(\mathbf{z}_{s(i)} | \mathbf{z}_{t(i)}) = 1$

$$\begin{aligned} \mathcal{L}(\psi, \lambda) &= \sum_{\mathbf{x}_0} \alpha(\mathbf{x}_0, \mathbf{z}_{t(i)}) \sum_{\mathbf{z}_{s(i)}} p(\mathbf{z}_{s(i)} | \mathbf{z}_{t(i)}, \mathbf{x}_0) [\log p(\mathbf{z}_{s(i)} | \mathbf{z}_{t(i)}, \mathbf{x}_0) - \log q_\psi(\mathbf{z}_{s(i)} | \mathbf{z}_{t(i)})] \\ &\quad + \lambda \left(\sum_{\mathbf{z}_{s(i)}} q_\psi(\mathbf{z}_{s(i)} | \mathbf{z}_{t(i)}) - 1 \right) \end{aligned} \quad (22)$$

Stationary condition for each $\mathbf{z}_{s(i)}$:

$$\frac{\partial \mathcal{L}}{\partial \psi} = - \frac{\sum_{\mathbf{x}_0} \alpha(\mathbf{x}_0, \mathbf{z}_{t(i)}) p(\mathbf{z}_{s(i)} | \mathbf{z}_{t(i)}, \mathbf{x}_0)}{q_\psi(\mathbf{z}_{s(i)} | \mathbf{z}_{t(i)})} + \lambda = 0 \quad (23)$$

$$\implies q_\psi(\mathbf{z}_{s(i)} | \mathbf{z}_{t(i)}) = \frac{\sum_{\mathbf{x}_0} \alpha(\mathbf{x}_0, \mathbf{z}_{t(i)}) p(\mathbf{z}_{s(i)} | \mathbf{z}_{t(i)}, \mathbf{x}_0)}{\lambda} \quad (24)$$

Now we determine λ from the constraint

$$1 = \sum_{\mathbf{z}_{s(i)}} q_\psi(\mathbf{z}_{s(i)} | \mathbf{z}_{t(i)}) = \sum_{\mathbf{z}_{s(i)}} \frac{1}{\lambda} \sum_{\mathbf{x}_0} \alpha(\mathbf{x}_0, \mathbf{z}_{t(i)}) p(\mathbf{z}_{s(i)} | \mathbf{z}_{t(i)}, \mathbf{x}_0) \quad (25)$$

$$\iff \lambda = \sum_{\mathbf{z}_{s(i)}} \sum_{\mathbf{x}_0} \alpha(\mathbf{x}_0, \mathbf{z}_{t(i)}) p(\mathbf{z}_{s(i)} | \mathbf{z}_{t(i)}, \mathbf{x}_0) \quad (26)$$

Putting all together:

$$q_{\psi^*}(\mathbf{z}_{s(i)} | \mathbf{z}_{t(i)}) = \frac{\sum_{\mathbf{x}_0} \alpha(\mathbf{x}_0, \mathbf{z}_{t(i)}) p(\mathbf{z}_{s(i)} | \mathbf{z}_{t(i)}, \mathbf{x}_0)}{\sum_{\tilde{\mathbf{z}}_{s(i)}} \sum_{\mathbf{x}_0} \alpha(\mathbf{x}_0, \mathbf{z}_{t(i)}) p(\tilde{\mathbf{z}}_{s(i)} | \mathbf{z}_{t(i)}, \mathbf{x}_0)} \quad (27)$$

$$= \frac{p(\mathbf{z}_{s(i)} | \mathbf{z}_{t(i)}) \frac{q(\mathbf{z}_{s(i)})}{p(\mathbf{z}_{s(i)})}}{\sum_{\tilde{\mathbf{z}}_{s(i)}} p(\tilde{\mathbf{z}}_{s(i)} | \mathbf{z}_{t(i)}) \frac{q(\tilde{\mathbf{z}}_{s(i)})}{p(\tilde{\mathbf{z}}_{s(i)})}} \quad (28)$$

$$= \frac{p(\mathbf{z}_{s(i)} | \mathbf{z}_{t(i)}) \mathbb{E}_{\mathbf{x}_0 \sim p(\cdot | \mathbf{z}_{s(i)})} \left[\frac{q(\mathbf{x}_0)}{p(\mathbf{x}_0)} \right]}{\sum_{\tilde{\mathbf{z}}_{s(i)}} p(\tilde{\mathbf{z}}_{s(i)} | \mathbf{z}_{t(i)}) \mathbb{E}_{\mathbf{x}_0 \sim p(\cdot | \tilde{\mathbf{z}}_{s(i)})} \left[\frac{q(\mathbf{x}_0)}{p(\mathbf{x}_0)} \right]} \quad (29)$$

For 27 to 28 we show that $\sum_{\mathbf{x}_0} \alpha(\mathbf{x}_0, \mathbf{z}_{t(i)}) p(\mathbf{z}_{s(i)} | \mathbf{z}_{t(i)}, \mathbf{x}_0) = p(\mathbf{z}_{s(i)} | \mathbf{z}_{t(i)}) \frac{q(\mathbf{z}_{s(i)})}{p(\mathbf{z}_{s(i)})}$:

$$\sum_{\mathbf{x}_0} \alpha(\mathbf{x}_0, \mathbf{z}_{t(i)}) p(\mathbf{z}_{s(i)} | \mathbf{z}_{t(i)}, \mathbf{x}_0) = \sum_{\mathbf{x}_0} p(\mathbf{x}_0 | \mathbf{z}_{t(i)}) \frac{q(\mathbf{x}_0)}{p(\mathbf{x}_0)} p(\mathbf{z}_{s(i)} | \mathbf{z}_{t(i)}, \mathbf{x}_0) \quad (30)$$

$$= \sum_{\mathbf{x}_0} p(\mathbf{z}_{t(i)} | \mathbf{x}_0) \frac{p(\mathbf{x}_0)}{p(\mathbf{z}_{t(i)})} \frac{q(\mathbf{x}_0)}{p(\mathbf{x}_0)} \frac{p(\mathbf{z}_{t(i)} | \mathbf{z}_{s(i)}) \cdot p(\mathbf{z}_{s(i)} | \mathbf{x}_0)}{p(\mathbf{z}_{t(i)} | \mathbf{x}_0)} \quad (31)$$

$$= \frac{p(\mathbf{z}_{t(i)} | \mathbf{z}_{s(i)})}{p(\mathbf{z}_{t(i)})} \sum_{\mathbf{x}_0} q(\mathbf{x}_0) p(\mathbf{z}_{s(i)} | \mathbf{x}_0) = p(\mathbf{z}_{t(i)} | \mathbf{z}_{s(i)}) \frac{q(\mathbf{z}_{s(i)})}{p(\mathbf{z}_{t(i)})} \quad (32)$$

For 28 to 29 we show that $\frac{q(\mathbf{z}_{s(i)})}{p(\mathbf{z}_{s(i)})} = \mathbb{E}_{\mathbf{x}_0 \sim p(\cdot | \mathbf{z}_{s(i)})} [q(\mathbf{x}_0)/p(\mathbf{x}_0)]$:

$$\frac{q(\mathbf{z}_{s(i)})}{p(\mathbf{z}_{s(i)})} = \frac{\sum_{\mathbf{x}_0} q(\mathbf{z}_{s(i)} | \mathbf{x}_0) q(\mathbf{x}_0)}{p(\mathbf{z}_{s(i)})} \quad (33)$$

$$= \frac{\sum_{\mathbf{x}_0} q(\mathbf{z}_{s(i)} | \mathbf{x}_0) p(\mathbf{x}_0) r(\mathbf{x}_0)}{p(\mathbf{z}_{s(i)})} = \sum_{\mathbf{x}_0} \frac{p(\mathbf{z}_{s(i)} | \mathbf{x}_0) p(\mathbf{x}_0)}{p(\mathbf{z}_{s(i)})} r(\mathbf{x}_0) \quad (34)$$

$$= \sum_{\mathbf{x}_0} p(\mathbf{x}_0 | \mathbf{z}_{s(i)}) r(\mathbf{x}_0) = \mathbb{E}_{\mathbf{x}_0 \sim p(\cdot | \mathbf{z}_{s(i)})} [q(\mathbf{x}_0)/p(\mathbf{x}_0)] \quad (35)$$

B Guided τ -Sampling

In the experiments, we observe that the combination of top- n_{ratio} selection and the guidance weight γ can misallocate probability mass, potentially causing the diffusion process to collapse into a fully masked sequence at the final step. For instance, when the top- n_{ratio} is small, the denoiser tends to propose tokens that are highly likely to belong to the source domain, which

Algorithm 2: NAIVE GUIDED DENOISE STEP ($\mathbf{z}_t, t, \Delta t$)

Require: noisy sequence $\mathbf{z}_t \in \mathcal{V}^L$, time t , step $\Delta t > 0$, denoiser p_θ , ratio net r_ϕ , mask index m , guidance schedule $\gamma(\cdot)$, noise schedule $\sigma(\cdot)$
Ensure: updated sequence \mathbf{z}_s

- 1: $\sigma_t \leftarrow \sigma(t)$
- 2: $\log x_\theta \leftarrow p_\theta(\mathbf{z}_t, \sigma_t) \{L \times |\mathcal{V}| \text{ logits}\}$
- 3: $E \leftarrow \{\ell \in \{1, \dots, L\} : z_t^{(\ell)} = m\} \{\text{masked positions}\}$
- 4: $\mathbf{z}_s \leftarrow \mathbf{z}_t$
- 5: **for all** $\ell \in E$ **do**
- 6: **for all** $v \in \mathcal{V}$ **do**
- 7: $\tilde{\mathbf{z}} \leftarrow \mathbf{z}_t$
- 8: $\tilde{z}^{(\ell)} \leftarrow v$
- 9: $\log r[\ell, v] \leftarrow \log r_\phi(\tilde{\mathbf{z}}, \sigma_t)$
- 10: **end for**
- 11: $\log q^{\text{guided}}[\ell, :] \leftarrow \log x_\theta[\ell, :] + \gamma(t) \log r[\ell, :]$
- 12: $\pi^{(\ell)} \leftarrow \text{softmax}(\log q^{\text{guided}}[\ell, :])$
- 13: $z_s^{(\ell)} \sim \text{Cat}(\pi^{(\ell)})$
- 14: **end for**
- 15:
- 16: **return** \mathbf{z}_s

then receive negative logits from the guidance ratio network. This effect is especially pronounced in high-noise regions, where all tokens experience a reduction in their probability of being unmasked, though some are affected more than others. Consequently, the overall probability of unmasking decreases, while the probability of remaining masked is incorrectly increased. This leads to the issue of ending up with a higher number of masked positions in the final step. To mitigate this problem, we apply a position-independent normalization:

$$q_{\theta, \phi}^\gamma(\mathbf{z}_s = \mathbf{m} \mid \mathbf{z}_t) = p(\mathbf{z}_s = \mathbf{m} \mid \mathbf{z}_t) = p_{\mathbf{m}}, \quad \sum_{\mathbf{v} \in \mathcal{V} \setminus \{\mathbf{m}\}} q_{\theta, \phi}^\gamma(\mathbf{z}_s = \mathbf{v} \mid \mathbf{z}_t) = 1 - p_{\mathbf{m}},$$

which implies the renormalized update over non-mask tokens, thus stabilizing the denoising diffusion process.

$$q_{\theta, \phi}^\gamma(\mathbf{z}_s = \mathbf{v} \mid \mathbf{z}_t) = \frac{(1 - p_{\mathbf{m}}) p_\theta(\mathbf{z}_s = \mathbf{v} \mid \mathbf{z}_t) r_\phi(\mathbf{z}_s = \mathbf{v})^\gamma}{\sum_{\tilde{\mathbf{v}} \in \mathcal{V} \setminus \{\mathbf{m}\}} p_\theta(\mathbf{z}_s = \tilde{\mathbf{v}} \mid \mathbf{z}_t) r_\phi(\mathbf{z}_s = \tilde{\mathbf{v}})^\gamma} \quad \text{for all } \mathbf{v} \in \mathcal{V} \setminus \{\mathbf{m}\}.$$

We use this algorithm in the first experiments section.

C Training Details

The Code will be released upon acceptance. In this section, we briefly describe the training setup for reproducibility. All training networks share the same learning schedule, which includes cosine decay with warmup and a high learning rate of 3×10^{-4} . The Adam optimizer is used, and we apply a dropout rate of 0.1. The batch size is set to 256 across all training algorithms. The time-independent and time-dependent Classifier is trained with 0.1 label smoothing and 4000 gradient steps. Importantly, the classifier is trained with binary labels, where the target domain is labeled as zero and the source domain as one. The ratio network is trained with λ set to 0.1, as outlined in the following pseudo-algorithm 3.

For sample corruption, we use a log-linear schedule with $\sigma_{\max} = 20$ and $\sigma_{\min} = 0.0001$. The planner is trained following Algorithm 4, using the same training configuration as described above, except that it is trained for 100k update steps. On the held-out validation set from the source domain, the planner achieves an average accuracy of 70%. In high-noise regions, it becomes considerably more challenging for the planner to predict which positions will be correctly denoised, due to the high variability in token unmasking.

D Application to continuous-time Score-based Models

D.1 Background

(Campbell et al. 2022) introduces a continuous-time framework for discrete denoising models formulated as a continuous-time Markov chain (CTMC). Unlike the discrete-time setting of (Austin et al. 2023) with steps $t = 0, 1, \dots, T$, here $t \in [0, T]$ is continuous.

Algorithm 3: Training loop for the ratio network $r_\phi(x_t, t)$

Require: source data $p(x)$ and target data $q(x)$, frozen classifier $d_\omega : \mathcal{V}^L \rightarrow [0, 1]$,
frozen time-dependent classifier $d_\omega : \mathcal{V}^L, t \rightarrow [0, 1]$ forward kernel $\text{CORRUPT}(x_0, \sigma_t)$ with schedule $\sigma(t)$,
batch size b , learning rate η , regularizer rate λ

- 1: **repeat**
- 2: **Sample** mini-batch x_0 of size b **from** \mathbf{p} and **draw** $t \sim \text{Uniform}(0, 1)$
- 3: $x_t \leftarrow \text{CORRUPT}(x_0, \sigma(t))$ {forward diffusion}
- 4: $\mathcal{L}_{\text{guidance}} = \frac{1}{b} \sum \|r_\phi(x_t, t) - \frac{1 - d_\omega(x_0)}{d_\omega(x_0)}\|_2^2$ {Guidance loss}
- 5:
- 6: **Sample** mini-batch x_0 of size b **from** \mathbf{q} and **draw** $t \sim \text{Uniform}(0, 1)$
- 7: $x_t \leftarrow \text{CORRUPT}(x_0, \sigma(t))$ {forward diffusion}
- 8: $\mathcal{L}_{\text{cycle}} = \frac{1}{b} \sum \|r_\phi(x_t, t) - \frac{1 - d_\omega(x_t, t)}{d_\omega(x_t, t)}\|_2^2$ {Guidance loss}
- 9:
- 10: $\mathcal{L} = \mathcal{L}_{\text{guidance}} + \lambda \cdot \mathcal{L}_{\text{cycle}}$
- 11: $\psi \leftarrow \psi - \eta \nabla_\psi \mathcal{L}$ {gradient update}
- 12: **until** convergence
- 13:
- 14: **return** trained parameters ψ

Algorithm 4: Training loop for the planner $\rho_\vartheta(x_t, t)$

Require: training corpus \mathcal{D} , frozen source denoiser $x_\theta : \mathcal{V}^L \rightarrow \mathbb{R}^{L \times |\mathcal{V}|}$ (per-position logits/probs),
forward kernel $\text{CORRUPT}(x_0, \sigma(t))$ with schedule $\sigma(t)$, batch size b , learning rate η

- 1: **repeat**
- 2: **Sample** mini-batch x_0 of size b from \mathcal{D} ; draw $t \sim \text{Uniform}(0, 1)$
- 3: $x_t \leftarrow \text{CORRUPT}(x_0, \sigma(t))$ {(1) corrupt the sample}
- 4: $\log x_\theta \leftarrow x_\theta(x_t); \hat{x}_0 \leftarrow \arg \max \log x_\theta$ {(2) pass to source denoiser}
- 5: $M \leftarrow (x_t = [\text{MASK}]); y \leftarrow \mathbf{1}[\hat{x}_0 = x_0]$ {(3) where denoiser is correct (masked positions)}
- 6: $s \leftarrow \rho_\vartheta(x_t)$ {(4) planner logits per position}
- 7: $\mathcal{L} \leftarrow \text{BCEWithLogits}(s[M], y[M])$ {(5) loss over masked positions only}
- 8: $\vartheta \leftarrow \vartheta - \eta \nabla_\vartheta \mathcal{L}$ {gradient update}
- 9: **until** convergence
- 10:
- 11: **return** trained planner parameters ϑ

In this section, we switch notation. The forward kernel is $p_{t|s}(\mathbf{y}' | \mathbf{y}) := p(\mathbf{z}_t = \mathbf{y}' | \mathbf{z}_s = \mathbf{y})$, the backward kernel is $p_{s|t}(\mathbf{y}' | \mathbf{y}) := p(\mathbf{z}_s = \mathbf{y}' | \mathbf{z}_t = \mathbf{y})$, the noising kernel is $p_t(\mathbf{y} | \mathbf{x}) := p(\mathbf{z}_t = \mathbf{y} | \mathbf{x}_0 = \mathbf{x})$, and the true backward transition is $p(\mathbf{y}' | \mathbf{y}, \mathbf{x}) := p(\mathbf{z}_s = \mathbf{y}' | \mathbf{z}_t = \mathbf{y}, \mathbf{x}_0 = \mathbf{x})$. This CTMC formulation allows transitions at arbitrary times. The forward corruption is specified by a rate matrix $R_t \in \mathbb{R}^{|\mathcal{V}| \times |\mathcal{V}|}$, and the reverse process by a reverse rate matrix \tilde{R}_t :

$$\begin{aligned} p_{t|s}(\mathbf{y}' | \mathbf{y}) &= \delta_{\mathbf{y}', \mathbf{y}} + R_t(\mathbf{y}', \mathbf{y}) \Delta t + \mathcal{O}(\Delta t^2), \\ p_{s|t}(\mathbf{y}' | \mathbf{y}, \mathbf{x}) &= \delta_{\mathbf{y}', \mathbf{y}} + \tilde{R}_t(\mathbf{y}', \mathbf{y}) \Delta t + \mathcal{O}(\Delta t^2). \end{aligned}$$

Here Δt denotes a small time increment when discretizing the continuous-time process, with $s = t - \Delta t$. Here, $\delta_{i,j}$ denotes the Kronecker delta (equal to 1 if $i = j$ and 0 otherwise), and $\mathcal{O}(\Delta t^2)$ denotes terms of order Δt^2 or higher. The reverse rate can be written in terms of the forward rate and the marginals $q_t(\cdot | \mathbf{x})$:

$$\tilde{R}_t(\mathbf{y}', \mathbf{y}) = \begin{cases} \frac{q_t(\mathbf{y}' | \mathbf{x})}{q_t(\mathbf{y} | \mathbf{x})} R_t(\mathbf{y}, \mathbf{y}'), & \mathbf{y}' \neq \mathbf{y}, \\ -\sum_{\tilde{\mathbf{y}} \neq \mathbf{y}} \frac{q_t(\tilde{\mathbf{y}} | \mathbf{x})}{q_t(\mathbf{y} | \mathbf{x})} R_t(\mathbf{y}, \tilde{\mathbf{y}}), & \mathbf{y}' = \mathbf{y}. \end{cases}$$

Concrete score. We can express the reverse process in terms of the forward transition rates and a *concrete score* defined by $s_\theta(\mathbf{y})_{\mathbf{y}'} \approx \frac{q_t(\mathbf{y}' | \mathbf{x})}{q_t(\mathbf{y} | \mathbf{x})}$, parameterized by a neural network $s_\theta : \mathcal{V} \rightarrow \mathbb{R}_{>0}^{|\mathcal{V}|}$. This enables training via concrete score matching (CSM) (Meng et al. 2023), directly analogous to score-based models in continuous domains (Song et al. 2021). (Lou, Meng, and Ermon 2024) propose the diffusion-weighted denoising score entropy (DWDSE) loss (their CDM-based objective) and note it can also be derived from the continuous-time likelihood framework of (Campbell et al. 2022); a detailed derivation appears in Appendix C.3 of (Sahoo et al. 2024). Concretely,

$$\lim_{T \rightarrow \infty} \mathbb{E}_{t \in \{\frac{1}{T}, \frac{2}{T}, \dots, 1\}} [\text{D}_{\text{KL}}(p_{s|t}(\mathbf{y}' | \mathbf{y}, \mathbf{x}) \| p_{s|t}(\mathbf{y}' | \mathbf{y}))] \quad (36)$$

$$= \mathbb{E}_{t \in [0,1]} \left[\sum_{\mathbf{y}' \neq \mathbf{y}} R_t(\mathbf{y}, \mathbf{y}') \left(s_\theta(\mathbf{y})_{\mathbf{y}'} - \frac{q_t(\mathbf{y}' | \mathbf{x})}{q_t(\mathbf{y} | \mathbf{x})} \log s_\theta(\mathbf{y})_{\mathbf{y}'} + K\left(\frac{q_t(\mathbf{y}' | \mathbf{x})}{q_t(\mathbf{y} | \mathbf{x})}\right) \right) \right], \quad (37)$$

where $K(a) = a \log a - a$.

D.2 Theorem

In the previous section, we introduced the diffusion process and the source-domain objective on which the score function s_θ is trained. We now state a theorem that enables sampling from the target distribution *without* retraining s_θ under the objective in 37. Let $r_\phi(\mathbf{y})$ denote the learned density-ratio guidance term defined earlier.

Theorem 3 (Score-Based Ratio Transfer Learning) *Let $s_\theta(\mathbf{y})_{\mathbf{y}'}$ be a score-based model trained on the source distribution p , and let $\tilde{R}_t^\theta(\cdot, \cdot)$ be the reverse-rate matrix induced by s_θ . Then, sampling from the target distribution q is given by the target reverse-rate matrix:*

$$\tilde{R}_t^\psi(\mathbf{y}', \mathbf{y}) = \begin{cases} \frac{r_\phi(\mathbf{y}')}{r_\phi(\mathbf{y})} \tilde{R}_t^\theta(\mathbf{y}', \mathbf{y}), & \mathbf{y}' \neq \mathbf{y}, \\ -\sum_{\tilde{\mathbf{y}} \neq \mathbf{y}} \frac{r_\phi(\tilde{\mathbf{y}})}{r_\phi(\mathbf{y})} \tilde{R}_t^\theta(\tilde{\mathbf{y}}, \mathbf{y}), & \mathbf{y}' = \mathbf{y}. \end{cases} \quad (38)$$

D.3 Proof of Theorem 3

For the proof, we take the loss for a small step Δt with $s = t - \Delta t$ from (36) and apply Theorem 1, which yields the following expression:

$$q_{s|t}^{\psi^*}(\mathbf{y}' | \mathbf{y}) = \frac{p_{s|t}(\mathbf{y}' | \mathbf{y}) \mathbb{E}_{\mathbf{x} \sim p(\cdot | \mathbf{y}')} \left[\frac{q(\mathbf{x})}{p(\mathbf{x})} \right]}{\sum_{\tilde{\mathbf{y}}} p_{s|t}(\tilde{\mathbf{y}} | \mathbf{y}) \mathbb{E}_{\mathbf{x} \sim p(\cdot | \tilde{\mathbf{y}})} \left[\frac{q(\mathbf{x})}{p(\mathbf{x})} \right]} \quad (39)$$

$$= \frac{p_{s|t}(\mathbf{y}' | \mathbf{y}) r_\phi(\mathbf{y}')}{\sum_{\tilde{\mathbf{y}}} p_{s|t}(\tilde{\mathbf{y}} | \mathbf{y}) r_\phi(\tilde{\mathbf{y}})} \quad (40)$$

We can already assume that the source backward kernel is approximated by $p_{s|t}(\mathbf{y}' | \mathbf{y}) = \delta_{\mathbf{y}', \mathbf{y}} + \tilde{R}_t^\theta(\mathbf{y}', \mathbf{y}) \Delta t + \mathcal{O}(\Delta t^2)$:

$$q_{s|t}^\psi(\mathbf{y}' | \mathbf{y}) = \frac{[\delta_{\mathbf{y}', \mathbf{y}} + \tilde{R}_t^\theta(\mathbf{y}', \mathbf{y}) \Delta t] r_\phi(\mathbf{y}')}{\sum_{\tilde{\mathbf{y}}} [\delta_{\tilde{\mathbf{y}}, \mathbf{y}} + \tilde{R}_t^\theta(\tilde{\mathbf{y}}, \mathbf{y}) \Delta t] r_\phi(\tilde{\mathbf{y}})} + \mathcal{O}(\Delta t^2)$$

We simplify the denominator by using the Taylor expansion of $1/(1+v)$ around $v=0$: $[\frac{1}{1+v} = 1 - v + \mathcal{O}(v^2)]$ and replacing $S := \sum_{\tilde{\mathbf{y}}} \tilde{R}_t^\theta(\tilde{\mathbf{y}}, \mathbf{y}) r_\phi(\tilde{\mathbf{y}})$:

$$\frac{1}{\sum_{\tilde{\mathbf{y}}} [\delta_{\tilde{\mathbf{y}}, \mathbf{y}} + \tilde{R}_t^\theta(\tilde{\mathbf{y}}, \mathbf{y}) \Delta t] r_\phi(\tilde{\mathbf{y}})} = \frac{1}{r_\phi(\mathbf{y}) + \Delta t S} = \frac{1}{r_\phi(\mathbf{y})} \left(1 + \frac{\Delta t S}{r_\phi(\mathbf{y})}\right)^{-1} = \frac{1}{r_\phi(\mathbf{y})} - \frac{\Delta t S}{r_\phi(\mathbf{y})^2} + \mathcal{O}(\Delta t^2)$$

1. For the Off-diagonal case $\mathbf{y}' \neq \mathbf{y}$, hence $\delta_{\mathbf{y}', \mathbf{y}} = 0$:

$$\begin{aligned} q_{s|t}^\psi(\mathbf{y}' | \mathbf{y}) &= \frac{[\delta_{\mathbf{y}', \mathbf{y}} + \tilde{R}_t^\theta(\mathbf{y}', \mathbf{y}) \Delta t] r_\phi(\mathbf{y}')}{\sum_{\tilde{\mathbf{y}}} [\delta_{\tilde{\mathbf{y}}, \mathbf{y}} + \tilde{R}_t^\theta(\tilde{\mathbf{y}}, \mathbf{y}) \Delta t] r_\phi(\tilde{\mathbf{y}})} + \mathcal{O}(\Delta t^2) \\ &= \tilde{R}_t^\theta(\mathbf{y}', \mathbf{y}) r_\phi(\mathbf{y}') \Delta t \left(\frac{1}{r_\phi(\mathbf{y})} - \frac{\Delta t S}{r_\phi(\mathbf{y})^2} + \mathcal{O}(\Delta t^2) \right) \\ &= \frac{\tilde{R}_t^\theta(\mathbf{y}', \mathbf{y}) r_\phi(\mathbf{y}')}{r_\phi(\mathbf{y})} \Delta t + \mathcal{O}(\Delta t^2), \end{aligned}$$

2. For the diagonal case $\mathbf{y}' = \mathbf{y}$:

$$\begin{aligned} q_{s|t}^\psi(\mathbf{y} | \mathbf{y}) &= \frac{[1 + \tilde{R}_t^\theta(\mathbf{y}, \mathbf{y}) \Delta t] r_\phi(\mathbf{y})}{r_\phi(\mathbf{y}) + \Delta t S} + \mathcal{O}(\Delta t^2) = \frac{1 + \tilde{R}_t^\theta(\mathbf{y}, \mathbf{y}) \Delta t}{1 + \frac{\Delta t S}{r_\phi(\mathbf{y})}} + \mathcal{O}(\Delta t^2) \\ &= \left(1 + \tilde{R}_t^\theta(\mathbf{y}, \mathbf{y}) \Delta t\right) \left(1 - \frac{\Delta t S}{r_\phi(\mathbf{y})}\right) + \mathcal{O}(\Delta t^2) = 1 + \left[\tilde{R}_t^\theta(\mathbf{y}, \mathbf{y}) - \frac{S}{r_\phi(\mathbf{y})}\right] \Delta t + \mathcal{O}(\Delta t^2). \end{aligned}$$

Putting these two cases together, we arrive at the following:

$$\begin{aligned} q_{s|t}^\psi(\mathbf{y}' | \mathbf{y}) &= \delta_{\mathbf{y}', \mathbf{y}} \left[1 + \left(\tilde{R}_t^\theta(\mathbf{y}, \mathbf{y}) - \sum_{\tilde{\mathbf{y}}} \tilde{R}_t^\theta(\tilde{\mathbf{y}}, \mathbf{y}) \frac{r_\phi(\tilde{\mathbf{y}})}{r_\phi(\mathbf{y})}\right) \Delta t\right] + (1 - \delta_{\mathbf{y}', \mathbf{y}}) \left[\tilde{R}_t^\theta(\mathbf{y}', \mathbf{y}) \frac{r_\phi(\mathbf{y}')}{r_\phi(\mathbf{y})} \Delta t\right] + \mathcal{O}(\Delta t^2) \\ &= \delta_{\mathbf{y}', \mathbf{y}} + \Delta t \left[\tilde{R}_t^\theta(\mathbf{y}', \mathbf{y}) \frac{r_\phi(\mathbf{y}')}{r_\phi(\mathbf{y})} - \delta_{\mathbf{y}', \mathbf{y}} \sum_{\tilde{\mathbf{y}}} \tilde{R}_t^\theta(\tilde{\mathbf{y}}, \mathbf{y}) \frac{r_\phi(\tilde{\mathbf{y}})}{r_\phi(\mathbf{y})}\right] + \mathcal{O}(\Delta t^2), \\ &= \delta_{\mathbf{y}', \mathbf{y}} + \Delta t \tilde{R}_t^\psi(\mathbf{y}', \mathbf{y}) + \mathcal{O}(\Delta t^2). \end{aligned}$$

Thus concluding the proof.

$$\tilde{R}_t^\psi(\mathbf{y}', \mathbf{y}) := \tilde{R}_t^\theta(\mathbf{y}', \mathbf{y}) \frac{r_\phi(\mathbf{y}')}{r_\phi(\mathbf{y})} - \delta_{\mathbf{y}', \mathbf{y}} \frac{1}{r_\phi(\mathbf{y})} \sum_{\tilde{\mathbf{y}}} \tilde{R}_t^\theta(\tilde{\mathbf{y}}, \mathbf{y}) r_\phi(\tilde{\mathbf{y}}).$$

The work from (Nisonoff et al. 2025) in equation (2) arrives at a similar term just for classifier-based guidance.